

Seismic Tests of Steel Buckling-Restrained Braced Frames for Evaluating Effects of Free-Edge Stiffeners and Frame Action Forces on Corner Gusset Connections



Chung-Che Chou

*Professor, Dept. of Civil Engineering, National Taiwan University, Taiwan. cechou@ntu.edu.tw
Researcher, National Center for Research on Earthquake Engineering, Taiwan.*

Jia-Hau Liu

Graduate Student Researcher, Dept. of Civil Engineering, National Taiwan University, Taiwan.

SUMMARY

This paper presents mechanics and cyclic test results of one-story one-bay buckling-restrained braced frames (BRBFs) with a single diagonal sandwiched BRB and corner gusset connections. Several BRBF tests focused on evaluating (1) the seismic performance of the BRB, (2) the effects of free-edge stiffeners and single/dual gusset configurations on the corner gusset behavior, and (3) the frame and brace action forces in the corner gusset. The BRBFs during tests performed well up to a drift of 2.5% with a maximum axial strain of 1.7% in the BRB. Without free-edge stiffeners, the single corner gusset plate buckled at a significantly low strength. The buckling could be eliminated by using dual corner gusset plates similar in size to the single gusset plate. At low drifts, the frame action force on the corner gusset was of the same magnitude as the BRB force. At high drifts, however, the frame action force significantly increased and caused weld fractures at column-to-gusset edges.

Keywords: *Steel buckling-restrained braced frame, Frame action force, Dual-gusset plate connection*

1. INTRODUCTION

Buckling-restrained braced frames (BRBFs) have been increasingly used for lateral load resistance in recent years. A BRBF differs from a conventionally braced frame because a buckling-restrained brace (BRB) yields under tension and compression without overall buckling. A BRB also differs from a new steel dual-core self-centering brace which provides both energy dissipation and re-centering properties to braced frames (Chou and Chen 2012, Chou et al. 2012). Gusset plates, which are commonly used in conventionally braced frames, are adopted in BRBFs to connect a BRB to the beam and column. The AISC Seismic Provisions (2005) require that axial capacity of a gusset plate exceed the ultimate load of a BRB to ensure stable energy dissipation. Based on the work by Bjorhovde and Chakrabarti (1985) and Gross (1990), Whitmore's width concept (1952) and formula for column buckling are adopted in AISC Specification (2005) for evaluating the tension and compression capacities of a corner gusset plate. The AISC Seismic Provisions also require that gusset plate instability be considered because recent studies demonstrated out-of-plane buckling or fractures of gusset plates prior to reaching the ultimate compression capacity of a BRB (Aiken et al. 2002, Tsai et al. 2008, Chou and Chen 2009). Moreover, Aiken et al. (2002) and Kasai et al. (2009) noted that when a diagonal BRB is used in a frame structure, a corner gusset plate is subjected to brace action and frame action such that the gusset-to-column tip or gusset-to-beam tip fractures when a BRB is under compression. This behavior is consistent with findings reported by Williams and Richard (1996), who demonstrated from a finite element model that a braced frame which does not incorporate framing members cannot simulate the pinching action (frame action) on a corner gusset plate.

This work presents mechanics of the corner gusset plate connection in the BRBF (Chou et al. 2011, Chou and Liu 2012). The objective is to develop a method to evaluate frame action and brace action forces on the corner gusset plate connections. The uniform force method and equivalent strut method, which can be used to estimate forces acting on a corner gusset plate, are applied for analysis. To verify the proposed method, cyclic tests are conducted on full-scale, one-story BRBFs, which use a sandwiched BRB and corner gusset plates. Chou and Chen (2010) have demonstrated stable hysteretic responses of the sandwiched BRBs up to a core axial strain of 2.6%; the core of the BRB if damaged in earthquake loading can be easily replaced without damaging restraining members. The BRB is

adopted in the braced frame, and five gusset configurations, which use either a single-gusset plate or dual-gusset plates as connections, are designed by considering brace and frame action forces in the corner gusset. Compared to a single-gusset-plate connection, dual gusset plates sandwiching a BRB core reduce gusset plate size, eliminate the need for splice plates, and enhance connection stability under compression (Chou et al. 2012). Calibrating the cyclic responses of the BRBF and the moment-resisting frame (MRF) subassemblies during the tests obtains the BRB axial force and displacement, leading to performance evaluations of the BRB and corner gusset connections.

2. MECHANICS OF CORNER GUSSET PLATE CONNECTIONS IN THE BRBF

2.1 Brace Action Force

Figure 1 shows a schematic diagram of the BRBF under lateral deformation. When a BRB is in tension, the angle of the beam-to-column connection θ_2 is smaller than the original angle θ_1 , producing compression forces F_g at the corner gusset edges (Figure 2(a)). When a BRB is in compression, the angle of the beam-to-column connection θ_3 exceeds the original angle θ_1 , producing tension forces F_g at the gusset edges (Figure 2(b)).

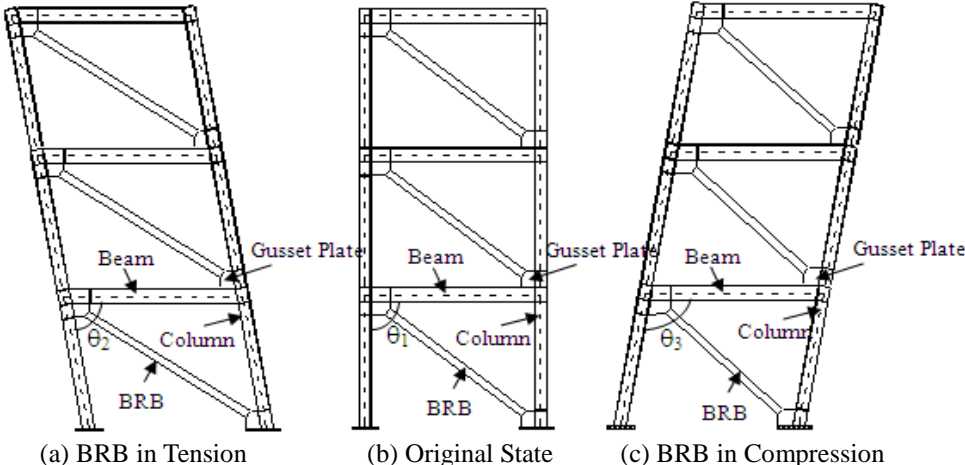


Figure 1. Deformation of a BRBF

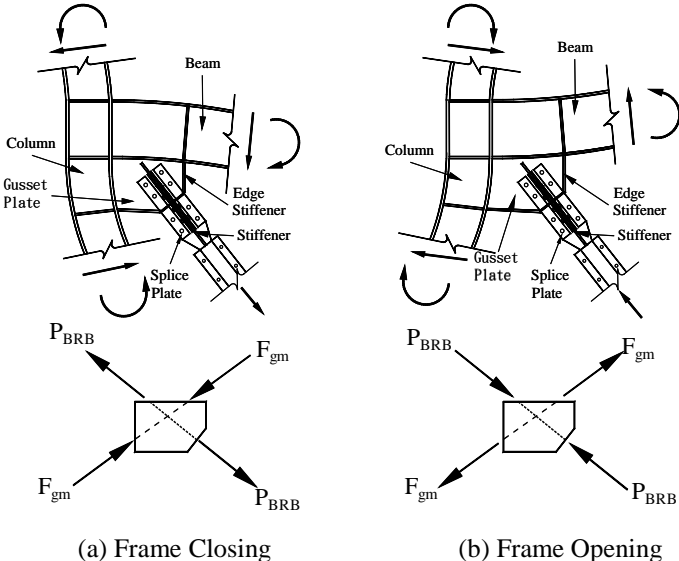


Figure 2. Frame and brace action in the gusset plate

Figure 3 shows a subassembly consisting of a beam, column, and corner gusset plate. The free-body diagram of the corner gusset plate includes the effects of brace action (Figure 3(c)) and frame action (Figure 3(d)). The uniform force method (Thornton 1991) determines the force components caused by brace action acting on the gusset-to-beam interface (N_b , Q_b) and gusset-to-column interface (N_c , Q_c):

$$N_b = \frac{e_b}{r} P_{BRB}, N_c = \frac{e_c}{r} P_{BRB}, Q_b = \frac{\alpha}{r} P_{BRB}, Q_c = \frac{\beta}{r} P_{BRB} \quad (1)$$

where e_b is the one-half beam depth; e_c is the one-half column depth; α is the distance from the column face to the centroid of the gusset-to-beam interface; β is the distance from the beam flange face to the centroid of the gusset-to-column interface, and $r = \sqrt{(\alpha + e_c)^2 + (\beta + e_b)^2}$.

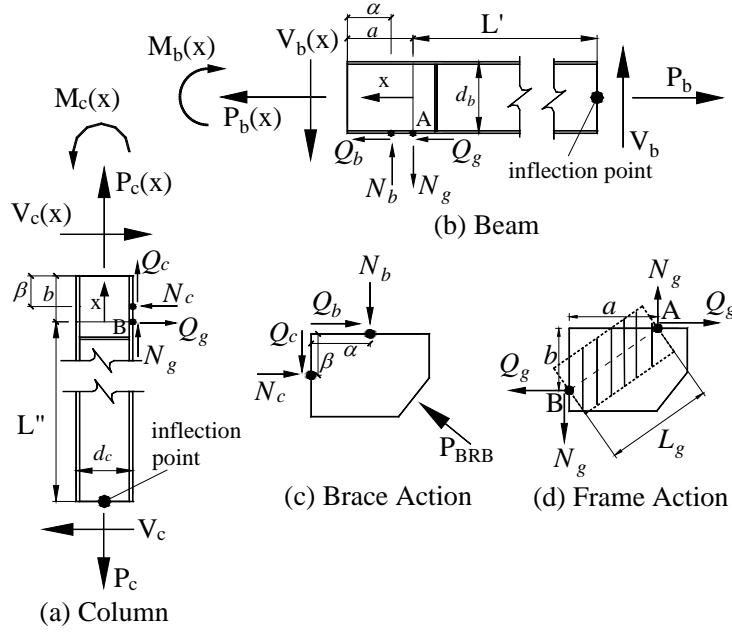


Figure 3. Free-body diagrams and strut deformation

2.2 Frame Action Force

An equivalent strut model, which considers frame action in the corner gusset plate, is used to determine force components N_g and Q_g acting on the gusset-to-beam and gusset-to-column interfaces (Figure 3). Axial stiffness, k_g , of an equivalent strut AB is defined as

$$k_g = \frac{b_e \times t \times E}{L_g} = \frac{t \times E}{2} \quad (2)$$

where E is the elastic modulus of steel; t is the gusset plate thickness; $b_e (=L_g/2)$ is the effective strut width (Lee 2002), and L_g is the strut length.

The beam moment $M_b(x)$ and axial force $P_b(x)$ from $0 \leq x \leq a - \alpha$ (Figure 3(b)), which consider the effects of frame action, are

$$M_b(x) = V_b(L'+x) - N_g x - Q_g \frac{d_b}{2} \quad (3)$$

$$P_b(x) = P_b - Q_g \quad (4)$$

where V_b is beam shear; P_b is beam axial force at the inflection point; L' is the distance from point A (strut end) to the beam inflection point; d_b is the beam depth, and $a (=0.6L_{gb})$ is the distance from the column face to point A, which was verified from the finite element analysis (Chou and Liu 2012). The beam moment $M_b(x)$ and axial force $P_b(x)$ from $a - \alpha \leq x \leq a$, which consider the effects of brace and frame actions, are

$$M_b(x) = V_b(L'+x) - N_g x - Q_g \frac{d_b}{2} + N_b[x - (a - \alpha)] - Q_b \frac{d_b}{2} \quad (5)$$

$$P_b(x) = P_b - (Q_g + Q_b) \quad (6)$$

The horizontal component of beam deformation at point A (Figure 3(b)) is obtained by integrating the axial strain of the beam bottom flange as follows:

$$\begin{aligned} d_{x,b} &= \int_0^a \frac{M_b(x)}{EI_b} \frac{d_b}{2} dx + \int_0^a \frac{P_b(x)}{EA_b} dx \\ &= \frac{d_b}{2EI_b} \left\{ V_b \left(L'a + \frac{a^2}{2} \right) - Q_g \left(\frac{ab + ad_b}{2} \right) + N_b \left[\frac{a^2 - (a - \alpha)^2}{2} - (a - \alpha)\alpha \right] - Q_b \frac{d_b}{2} \alpha \right\} \\ &\quad + \frac{1}{EA_b} (P_b a - Q_g a - Q_b \alpha) \end{aligned} \quad (7)$$

where I_b is the beam moment of inertia and A_b is the beam cross-sectional area. Following the same steps, the vertical component of column deformation at point B (Figure 3(a)), $d_{x,c}$, is obtained by integrating the axial strain of the column flange. Based on the horizontal and vertical deformation components of the strut, $d_{x,b}$ and $d_{x,c}$, the elongation of the equivalent strut δ is

$$\delta = \delta_1 + \delta_2 \approx \frac{L_g}{a} d_{x,b} + \frac{L_g}{b} d_{x,c} \quad (8)$$

where δ_1 is the strut axial deformation near the gusset-to-beam interface, and δ_2 is the strut axial deformation near the gusset-to-column interface. The axial elongation of the equivalent strut can also be established by considering the axial force F_{gm} and axial stiffness k_g in the strut. Rearranging equations (2), (7), and (8), the strut axial force, F_{gm} , caused by beam shear, V_b , and column shear, V_c , is (Chou and Liu 2012):

$$F_{gm} = A' \{ C_1 \times V_b + C_2 \times V_c \} \quad (9)$$

where

$$A' = \frac{L_g}{a \left\{ \frac{1}{ak_g} + \frac{d_b}{2EI_b} \left(\frac{b + d_b}{2} \right) + \frac{d_c}{2EI_c} \left(\frac{b}{2} + \frac{bd_c}{2a} \right) \right\}} \quad (10)$$

$$C_1 = \frac{d_b}{2EI_b} \left(L' + \frac{a}{2} \right) \quad (11)$$

$$C_2 = \frac{d_c}{2EI_c} \left(L'' + \frac{b}{2} \right) \quad (12)$$

where L_g is the strut length, I_b is the moment of inertia of beam, I_c is the moment of inertia of column, L' is the distance from strut end (point A) to the beam inflection point, L'' is the distance from strut end (point B) to the column inflection point, d_b is the beam depth, d_c is the column depth, a ($=0.6L_{gb}$) is the distance from the column face to point A, b ($=0.6L_{gc}$) is the distance from the beam flange face to point B, and L_{gb} and L_{gc} are the gusset dimensions.

From the pushover analysis of the BRBF, the BRB force and shears in the beam and column give the force components in the corner gusset caused by brace action (P_{BRB}) and frame action (F_{gm}). Adding stresses produced by frame action and brace action gives the maximum normal stress, $\sigma_{\max,b}$, and maximum shear stress, $\tau_{\max,b}$, at the gusset tip. The von-Mises stress at the gusset tip is

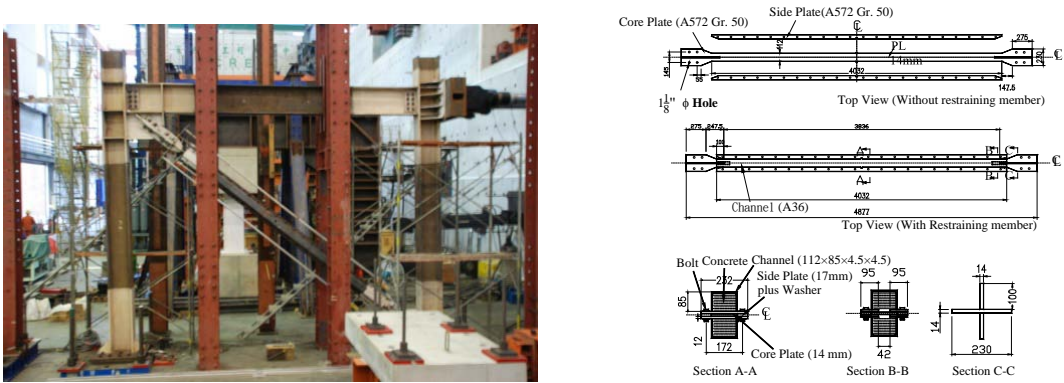
$$\bar{\sigma} = \sqrt{\sigma_{\max,b}^2 + 3\tau_{\max,b}^2} \leq F_y \quad (13)$$

The gusset and free-edge stiffener size can be determined by limiting von-Mises stress less than the yield strength of steel at a design drift (i.e. 1%).

3. CORNER GUSSET PLATE SPECIMEN

Figure 4(a) shows the frame subassembly, which uses a single-diagonal BRB (Figure 4(b)) to dissipate seismic energy. Five different corner gusset connections (Specimens 1-5) were used to connect the BRB and framing members. Specimens 1 and 2 had a typical single gusset configuration and Specimens 3-5 had a dual gusset configuration. Free-edge stiffeners, 200 mm wide rectangular plates, were used in Specimens 1 and 3. Specimen 1 used a typical single-gusset plate connection, which had a 14-mm-thick gusset plate and two 12-mm-thick free-edge stiffeners, welded to the gusset plate and beam or column. Both ends of the BRB stopped between the top and bottom corner gusset plates, and eight splice plates with 25-mm diameter A490 bolts were used to connect the BRB and gusset plate. Specimen 2 was identical to Specimen 1 except that free-edge stiffeners were not used in Specimen 2. Gusset size was generally determined by either compression capacity or by von-Mises stress at gusset tips, so the tensile capacity of the gusset calculated based on the Whitmore method exceeded the tensile capacity, T_{max} , of the BRB (Table 1(a)). The ultimate compression capacity of the single gusset plate calculated according to measured yield strength and the buckling coefficient $k=0.65$ was 1368 kN (Table 1(b)), which exceeded that of the BRB (914 kN). In Specimen 2, which was a single gusset plate without free-edge stiffeners, the ultimate compression capacity calculated using the buckling coefficient of $k=2$ was 759 kN, which was smaller than that of the BRB. This indicates that the single gusset plate without free-edge stiffeners would buckle before reaching the maximum compression capacity of the BRB. However, if the compression capacity was calculated using a buckling coefficient of $k=1.2$, compression capacity for Specimen 2 exceeded C_{max} of the BRB (Table 1(b)). Therefore, this specimen was used to test whether the AISC Specification (2005) for k is appropriate.

Specimens 3 to 5 used a pair of 8-mm thick gusset plates to connect the BRB and framing members. Specimen 3 was identical to Specimen 4 except that 12-mm thick free-edge stiffeners were only added in Specimen 3 (Figure 5(a)). Specimen 5 was identical to Specimen 4 except that the BRB was turned 90 degrees such that the weak axis of the core plate was transverse to the loading plane with the dual gusset plates spaced 170 mm apart (Figure 5(b)). The BRB ends in Specimens 3 and 4 were inserted into dual gusset plates; longitudinal fillet welds and 25-mm diameter bolts were used to connect dual gusset plates and the BRB. In Specimen 5, only fillet welds were used to connect the dual gusset plates and BRB. The moment of inertia was significantly larger in the dual gusset configuration than in a single gusset configuration of similar size, and the compression capacity of 5-mm thick dual gusset configuration (1566 kN and 1442 kN in Specimen 3 and 4 geometries, respectively) exceeded that of the BRB (914 kN). However, 8-mm thick dual gusset plates were used in Specimens 3-5 to limit maximum von-Mises stresses at gusset tips below yield strength F_y (Table 2). Except for Specimen 2, the von-Mises stresses at the gusset tips were smaller than gusset yield strength F_y obtained from the coupon test. The critical unbraced length of the unit strip, L_c , was negative in Specimen 5 details due to a negative value of L_{c1} (Figure 5(b)), indicating that buckling of the dual gusset plates could be excluded. In Specimens 2, 4, and 5, which lacked free-edge stiffeners, the effects of single or dual gusset plates on the BRB connection were evaluated.



(a) Test Setup (2% Drift)

(b) BRB Details (Chou and Chen 2010)

Figure 4. Test setup and BRB details

Table 1. Tensile and compression capacities of the gusset plate
(a) Tensile Capacity

Specimen	1	2	3	4	5
b_e (mm)	272	272	353	353	448
t_g (mm)	14	14	2×8	2×8	2×8
R_n (kN)	1466	1466	2530	2530	3211

(b) Compressive Capacity

Item	With Edge Stiffener		Without Edge Stiffener			
	$k=0.65$		$k=2.0$		$k=1.2$	
Specimen	1	3	2	4	5	2
b_e (mm)	272	353	272	353	448	272
L_c (mm)	183	174	183	174	-	183
P_{cr} (kN)	1368	2506	759	2312	-	1157

Table 2. Forces and stresses in the beam-to-gusset Edge (1% drift)

Specimen	F_{gm} (kN)	P_{BRB} (kN)	$\bar{\sigma}$ (MPa)	F_y (MPa)
1 ($t_g=14$ mm)	750	730	381	385
2 ($t_g=14$ mm)	750	730	427	385
3 ($t_g=2\times 8$ mm)	807	730	373	448
4 ($t_g=2\times 8$ mm)	807	730	412	448
5 ($t_g=2\times 8$ mm)	807	730	412	448

($V_b=170$ kN, $V_c=240$ kN)

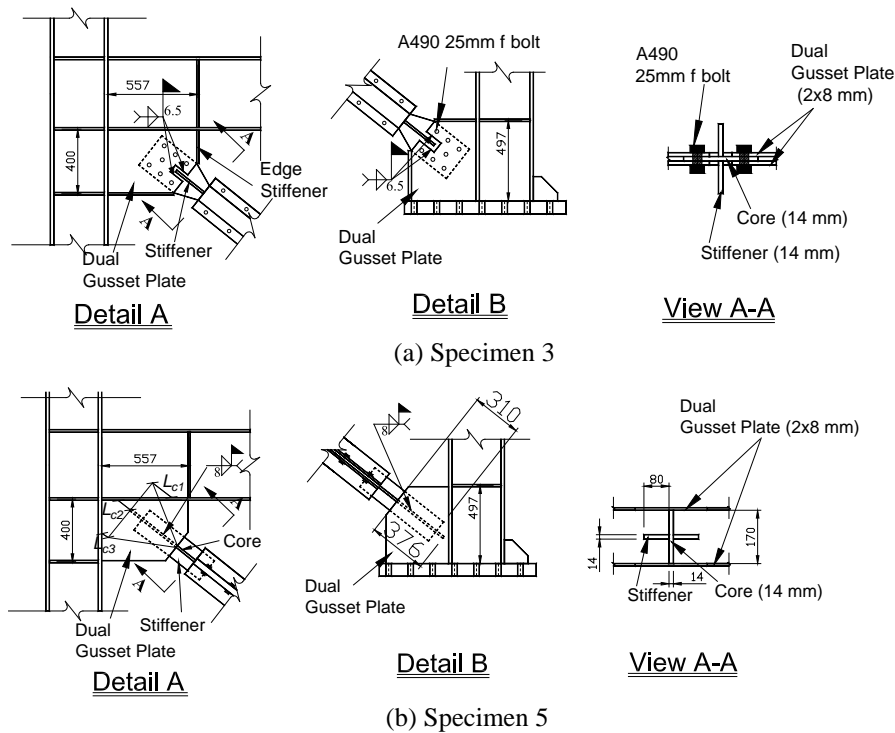


Figure 5. Dual gusset plate connection details

4. BRBF SUBASSEMBLY TEST

The BRBF subassembly was subjected to prescribed loading according to Section T6 of the AISC Seismic Provisions (2005) until specimen failure or until 2% drift was reached. The moment-resisting frame (MRF) was also tested to investigate its seismic performance after removing the BRB and corner gusset plates. Comparing the cyclic responses of the BRBF and MRF subassemblies evaluated the performance of the BRB with the corner gusset connection.

4.1 Test Results

4.1.1 Specimens 1 and 2

The BRBF subassembly had stable energy dissipation throughout the test except for Specimen 2 (Figure 6). The BRB generally began to yield around an interstory drift of 0.5%; column and beam yielding were observed at an interstory drift of 1%. In Specimen 1 test, the beam-to-gusset and column-to-gusset edge tips yielded at an interstory drift of 1.5%. At an interstory drift of 2%, neither the gusset nor the BRB buckled; however, in the moment connection near the actuator, the beam web top access hole fractured. A top cover plate and two side plates were utilized to rehabilitate the moment connection (Chou et al. 2010, Chou and Jao 2010) so that the frame subassembly could be re-used in further tests.

Free-edge stiffeners in Specimen 2 connection were removed from the gusset plate after completing the Specimen 1 test. The BRBF subassembly was re-tested with the same BRB and corner gusset plate. The top gusset plate buckled at an interstory drift of -0.63% when the BRB was in compression. The bottom gusset plate did not buckle. The BRBF maintained peak strength when the BRBF was displaced in the reverse direction to an interstory drift of 1% (Figure 6(b)). The out-of-plane deformation of the single gusset plate was significant at an interstory drift of -1% (Figure 7(a)). Since the peak lateral force at this drift level (-1%) decreased from 1220 kN (in Specimen 1 test) to 980 kN (in Specimen 2 test), the test was stopped. Two restraining members were removed from the BRB to inspect the core; the core revealed no fractures, and only one end of the BRB revealed flexural bending. Two stoppers located in the middle of the core unexpectedly fell off due to false fabrication by the manufacturer, which caused the restraining members to slide during the test. After re-fabricating the other two BRB cores to correct this defect, the BRBs were re-assembled with original restraining members.

4.1.2 Specimens 3 and 4

A new BRB with a dual gusset plate configuration and free-edge stiffeners (Specimen 3) was installed in the frame subassembly. As in Specimen 1 test, energy dissipation in the frame subassembly was stable throughout the Specimen 3 test (Figure 6(c)). Significant yielding was observed in dual gusset plates near the beam-to-gusset and column-to-gusset edge tips. After completing the Specimen 3 test, free-edge stiffeners were removed from the dual gusset plates, and the frame was re-tested with the same BRB and dual gusset plates (Specimen 4). Unlike Specimen 2, however, the dual gusset plates sustained maximum lateral force of 1720 kN at interstory drift of 2% without buckling (Figure 6(d) and Figure 7(b)), indicating that, without free-edge stiffeners, the out-of-plane stability is much better in a dual gusset plate configuration than in a single gusset plate configuration of similar size.

4.1.3 Specimen 5 and MRF

After removing the BRB and dual gusset plates, the MRF was tested to investigate its hysteretic behavior. The rehabilitated moment connection performed well up to an interstory drift of 2% (Figure 6(f)). The frame was then installed with a new BRB and Specimen 5 gusset details. The frame subassembly also had stable energy dissipation up to an interstory drift of 2%. However, a crack occurred at the beam bottom flange near the junction between the gusset tip and web stiffener while the frame subassembly was moved to an interstory drift of -2% (frame opening). Significant yielding was also observed near the bottom gusset tips, but no fractures were noted. Two additional cycles with 2.5% drift were conducted on this specimen frame. Weld fractures were observed in the top and bottom column-to-gusset interfaces at an interstory drift of -2.5% (Figure 7(c)). These cracks occurred

when the BRB was under compression and the frame subassembly opened as illustrated in Figure 2(b). These cracks closed when the BRB was under tension and the frame closed (2.5% drift). Strength was slightly reduced in the second cycle (Figure 6 (e)) due to beam buckling near the rehabilitated moment connection. These cracks might be eliminated at the extreme loading stage if free-edge stiffeners were incorporated in the gusset connection. Neither the gusset nor the BRB buckled in Specimen 5 test.

4.1.4 Gusset Plate Buckling Load

The axial displacement of the BRB was obtained by measuring the relative displacement at both ends of the BRB. In Specimen 2 test, the gusset plate buckled when the axial force in the BRB was 693 kN (Chou et al. 2011). This compression force was much smaller than the compression capacity of the gusset plate (1157 kN) calculated based on the elastic modulus, buckling coefficient $k=1.2$, and true yield strength of the steel in the buckling equation. However, the compression capacity of the gusset plate calculated based on the buckling coefficient $k=2$ was 758 kN, which was slightly larger than that observed in the test. This indicates that $k=2$ is better than $k=1.2$ when using the column strip method to estimate compression capacity of a gusset without free-edge stiffeners. Except for Specimens 1 and 2 connections, the compression-to-tension force ratios were around 1.1 and 1.2, which were lower than 1.3 specified by the AISC Seismic Provisions (2005). The ratio of Specimen 1 was larger than others due to sliding of the restraining member at high drifts.

4.2 Frame Action Force

The equivalent strut force in the gusset was compared to the axial force in the BRB. In each test, shears in the beam and column were determined based on rosette readings, the shear modulus of steel, and the cross-sectional area of the beam and column, respectively. The force in the BRB, P_{BRB} , was obtained from the BRBF and MRF test results (Figure 6). The equivalent strut forces F_{gm} computed using Eq. (9) were of the same order of the brace force before an interstory drift of 1% (Figure 8). Afterwards, the incremental change in force on the BRB was smaller than that in the equivalent strut because most beam and column sections remained in the elastic range whereas the BRB remained within the yield plateau range. Compared to the BRB, the frame exerted a larger force on the gusset at high drift levels, which caused the gusset edges to fracture.

4.3 Effects of Free-edge Stiffeners

Specimens 3 and 4 had the same gusset configuration except that Specimen 3 had free-edge stiffeners. Normal strains at the gusset tip did not vary remarkably in Specimen 3 but did increase with drift in Specimen 4. Shear strains in the gusset plate were similar in Specimens 3 and 4, indicating that free-edge stiffeners were ineffective in transferring shear forces from the brace to the beam.

5. CONCLUSIONS

This work presented mechanics and cyclic tests of BRBFs, which used corner gusset plates to connect the diagonal BRB and frame. The objectives were (1) to develop a method that can evaluate the effects of frame action and brace action on the corner gusset plate, and (2) to examine the cyclic performance of the single and dual gusset connections and the BRB. Five gusset configurations, utilizing either the single-gusset plate or dual-gusset plates, were designed by considering brace and frame action forces in the corner gusset. The following conclusions are based on the proposed mechanics and experimental results.

1. A BRB connection designed based on the frame and brace action forces exhibits stable energy dissipation up to an interstory drift of 2.5% with a maximum axial strain of 1.7% in the BRB. Compared to the dual gusset configuration, the single gusset configuration provides more direct transfer of forces because the beam web, gusset, and column web plates all exist in the co-plane. The dual gusset plate configuration which provides better out-of-plane stability compared to the single gusset configuration also show good behavior for a BRBF. In a single gusset configuration without free-edge stiffeners (Specimen 2), the gusset plate buckles at a low interstory drift. This does not occur in a dual gusset plate configuration (Specimen 4) of similar size. When free-edge

stiffeners are not adopted in gusset connections, a side-sway mode of gusset buckling can occur and the coefficient k when estimating compression capacity should be 2 rather than 1.2. Free-edge stiffeners can also reduce normal stresses at gusset tips and are needed for ensuring good behavior in the single gusset configuration.

- Although the corner gusset plate in the BRBF is subjected to both brace action and frame action forces, the latter is not considered in AISC Seismic Provisions (2005). In the corner gusset, forces caused by frame action and brace action are comparable at low interstory drifts. At high interstory drifts, however, the frame action force in excess of brace action force causes weld fractures at gusset tips under frame opening. In addition to checking tensile capacity and stability of gussets based on the BRB axial load, the proposed method is used to size gusset plates and free-edge stiffeners by considering both brace and frame action forces in gusset connections. This is needed especially for the dual-gusset plate configuration because the design is controlled by Eq. (13) and tensile capacity not buckling of the gusset plate.

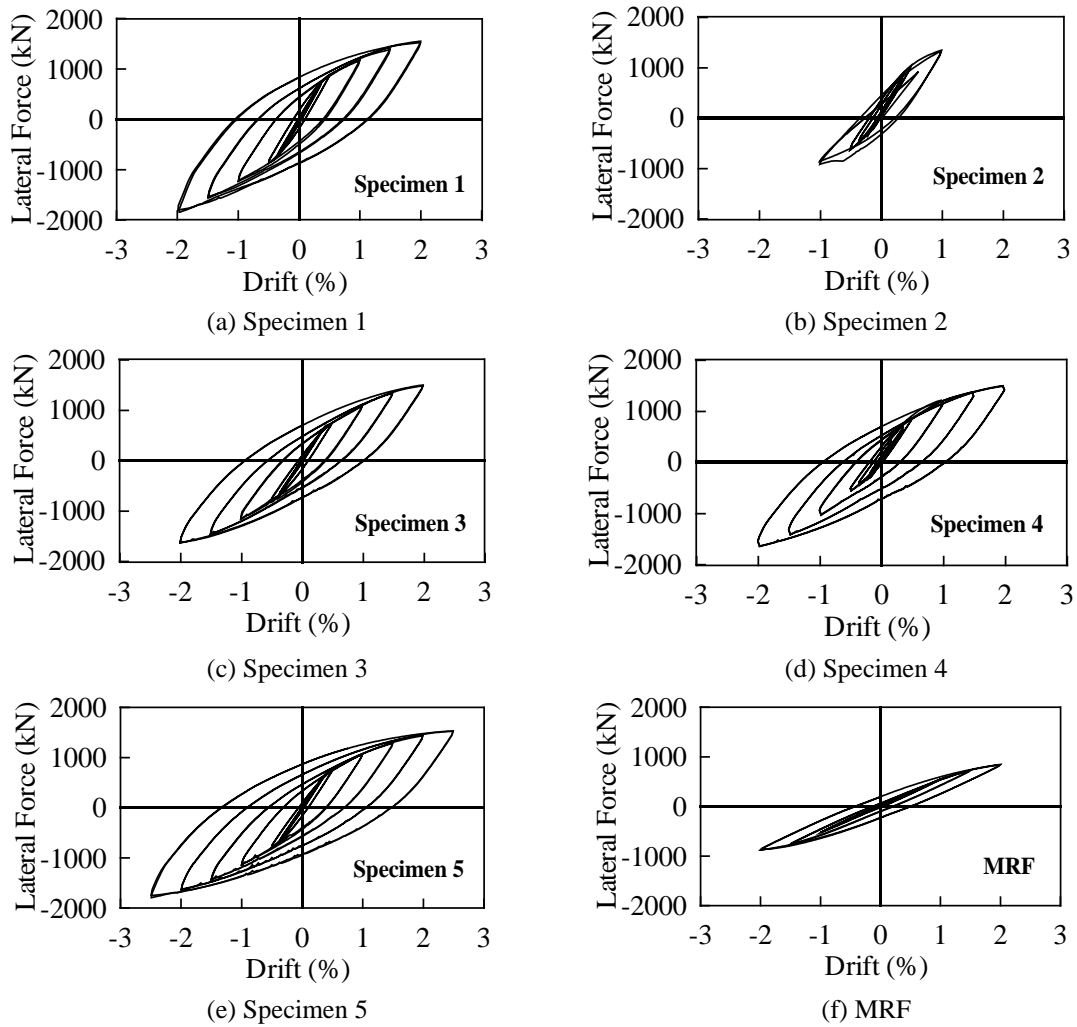


Figure 6. Lateral force versus story drift responses



(a) Specimen 2 (-1% drift) (b) Specimen 4 (-2% drift) (c) Specimen 5 (-2.5% drift)

Figure 7. Observed performance in BRBF subassembly test

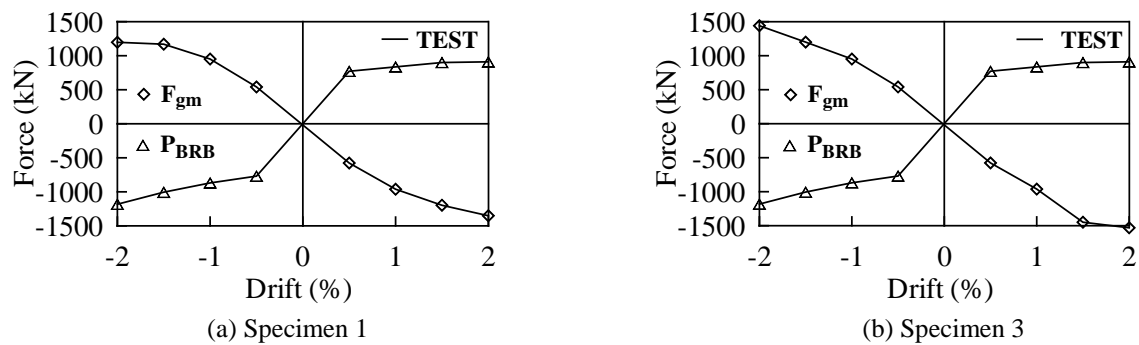


Figure 8. Frame action force versus brace action force in BRBF tests

ACKNOWLEDGMENTS

The authors would like to thank the National Science Council, Taiwan for financially supporting this research under Contract No. NSC 98-2625-M-002-017. The authors would also like to thank Prof. K. C. Tsai in providing valuable advices in the program.

REFERENCES

- AISC. (2005). *Seismic provisions for structural steel buildings*, American Institute of Steel Construction, IL.
- AISC. (2005). *Specification for structural steel buildings*. ANSI/AISC 360-05. American Institute of Steel Construction, Chicago, IL.
- Aiken ID, Mahin SA, and Uriz P. (2002). Large-scale testing of buckling-restrained braced frames. *Proceedings of Japan Passive Control Symposium*, 35-44, Tokyo Institute of Technology, Japan.
- Bjorhovde R. and Chakrabarti S.K. 1985. Tests of full size gusset plate connections. *J. Struct. Engrg.*, Vol. 111, No. 3, ASCE, 667-683.
- Chou C-C, Chen P-J. (2009). Compressive behavior of central gusset plate connections for a buckling-restrained braced frame. *J. Constructional Steel Research*, 65(5), 1138-1148.
- Chou C-C, Chen S-Y. (2010). Subassemblage tests and finite element analyses of sandwiched buckling-restrained braces. *Engineering Structures*, 32, 2108-2121.
- Chou C-C, Jao C-K. (2010). Seismic rehabilitation of welded steel beam-to-box column connections utilizing internal flange stiffeners. *Earthquake Spectra*, 26(4), 927-950.
- Chou C-C, Tsai K-C, Wang Y-Y, Jao C-K. (2010). Seismic rehabilitation performance of steel side plate moment connections. *Earthquake Engineering and Structural Dynamics*, 39, 23-44.
- Chou C-C, Liu J-H, Pham D-H. (2011). Steel buckling-restrained braced frames with single and dual corner gusset connections: seismic tests and analyses. *Earthquake Engineering and Structural Dynamics* (available on line 2011/10).
- Chou C-C, Liu J-H. (2012). Frame and brace action forces on steel corner gusset plate connections in buckling-restrained braced frames. EQS-112410EQS197M.3d, *Earthquake Spectra* (published in 2012/5).
- Chou C-C, Liou G-S, Yu J-C. (2012). Compressive behavior of dual-gusset-plate connections for buckling-restrained braced frames. doi:10.1016/j.jcsr.2012.03.003, *J. Constructional Steel Research* (available on line 2012/4).
- Chou C-C, Chen Y-C. (2012). Development of steel dual-core self-centering braces with E-glass FRP composite tendons: cyclic tests and finite element analyses. *The International Workshop on Advances in Seismic Experiments and Computations*, Nagoya, Japan.
- Chou C-C, Chen Y-C, Pham D-H, Truong V-M. (2012). Experimental and analytical validation of steel dual-core self-centering braces for seismic-resisting structures. *9th International Conference on Urban Earthquake Engineering/4th Asia Conference on Earthquake Engineering*, Tokyo, Japan.
- Gross JL. (1990). Experimental study of gusseted connections. *Engineering J.*, 3rd quarter, 89-97.
- Kasai K, Ooki Y, Ito H, Motoyui S, Hikino T, Sato E. (2009). Full-scale tests of passively-controlled 5-story steel building using E-defense shake table. *International Conference for Behavior of Steel Structures in Seismic Area*, Pennsylvania, USA.
- Lee CH. (2002). Seismic design of rib-reinforced steel moment connections based on equivalent strut model. *J. Struct. Engrg.*, ASCE., Vol. 128, No. 9, 1121-1129.
- Tsai K-C, Hsiao B-C, Wang K-J, Weng Y-T, Lin M-L, Lin K-C, Chen C-H, Lai J-W, Lin S-L. (2008). Pseudo-dynamic tests of a full scale CFT/BRB frame-Part I: Specimen design, experiment and analysis. *Earthquake Engineering and Structural Dynamics*, 37: 1081-1098.
- Thornton WA. (1991). On the analysis and design of bracing connections. *National Steel Construction Conference Proceedings*, AISC, 26.1-26.33, Chicago.
- Whitmore RE. (1952). Experimental investigation of stresses in gusset plate. Bulletin No. 16, Engineering Experiment Station, University of Tennessee.
- Williams GC., Richard RM. (1996). Analysis and design of large diagonal bracing connections. *Structural Engineering Review*, Vol. 8, No. 1, 1-27.